Applied Nanoscience (2022) 12:411–425
https://doi.org/10.1007/s13204-021-01682-1

ORIGINAL ARTICLE

Isomerization of linear hexane over acid-modified nanosized nickel-containing natural Ukrainian zeolites

L. K. Patrylak[1] · O. P. Pertko[1] · A. V. Yakovenko[1] · Yu. G. Voloshyna[1] · V. A. Povazhnyi[1] · M. M. Kurmach[2]

Received: 4 November 2020 / Accepted: 15 January 2021 / Published online: 6 February 2021

Abstract

Bifunctional catalysts on the basis of Ukrainian natural mordenite-clinoptilolite rocks modified by hydrochloric acid and by witness impregnation with nickel have been synthesized. Samples have been characterized by means of XRD, XRF, FTIR-spectroscopy, low temperature nitrogen adsorption/desorption, DTA/TG, TEM. Catalysts have been tested in micro pulse linear hexane isomerization. Hydrochloric acid treatment of natural zeolite rock leads to silica-to-alumina ratio increasing and raising the BET surface as well as the volumes of mesopores and micropores. The nickel nanoparticles deposited over zeolite crystals have a predominant size of 10 nm, but for some samples smaller ones of 5 nm and bigger ones of 20–50 nm have been found using TEM investigations. Pyridine sorption shows Brønsted and Lewis acidity of the catalysts, moreover the lower hydrochloric acid concentration using leads to practically equal Brønsted and Lewis acidity, the higher acid concentrations causes the Lewis acidity predominance. DTA/TG investigations show that water physically sorbed in the pores of the samples has been removed up to 200 °C from lager cavities of acid-treated catalysts and up to 500 °C from narrower cavities for untreated initial rock. Removing zeolite structure water up to 800 °C causes the dehydroxylation and Brønsted acidity transformation into Lewis acidity. The sample dealuminated by 1 mol dm^{-3} acid with nickel nanoparticles of 5–8 nm demonstrates the best performance in the isomerization of n-hexane. It is characterized by a 20% yield of hexane isomers at 250 °C and 70% selectivity.

Keywords Natural zeolite rock · Mordenite · Bifunctional catalyst · Hexane isomerization · Activity · Selectivity

Introduction

More and more scientists around the world are paying attention to the creation of new nanostructured materials, among them are micro/mesoporous zeolite-containing materials, which are of great importance (Na et al. 2013; Serrano and Pizzaro 2013; Liu et al. 2017; Bai et al. 2019). An advanced porous system is the key to creating highly efficient adsorbents and catalysts that will ensure the proper accessibility of reagents to the active sites (Mitchell et al. 2015; Feliczak-Guzik 2018; Khan et al. 2019; Weissenberger et al. 2019).

Problems with high diffusion rates of reagents or reaction products often occur for zeolite materials with high microporosity. As a result, the processes proceed in the intradiffusion region and the increase of catalyst activity becomes meaningless. Moreover, highly active compositions may lose their efficiency because of partial blocking of the active sites by overlapping narrow zeolite channels and pores with reagents or coke precursors (Nordvang et al. 2015; Devaraj et al. 2016; Liu et al. 2016; Patrylak and Pertko 2018). This moment is very relevant for large pores mordenite type zeolites with channel structure. Bigger channels of 0.7 nm diameter are generally available for hydrocarbon reagents, but smaller channels (0.3 nm) can adsorb predominantly water molecules. Therefore, the question of improving the porous system of mordenite zeolite, which is a base of an industrial catalyst for the isomerization of linear alkanes, is very relevant.

Modern isomerization catalysts are bifunctional systems, which, in addition to the acid component, contain hydrogenating-dehydrogenating metals. The latter is usually

✉ L. K. Patrylak
lkpg@ukr.net

[1] Department of Catalytic Synthesis, V.P.Kukhar Institute of Bioorganic Chemistry and Petrochemistry of NAS of Ukraine, Murmanska Str., 1, Kyiv-02094, Ukraine

[2] Department of Porous Compounds and Materials, L.V.Pysarzhevski Institute of Physical Chemistry of NAS of Ukraine, Prospect Nauky, 33, Kyiv-03028, Ukraine

represented by elements of the platinum group. A number of studies have shown high activity of both bimetallic systems containing nickel and platinum (Yoshioka et al. 2005; Jardao et al. 2007; Lima et al. 2011; Martins et al. 2013) as well as monometallic nickel containing MFI zeolites (Patrylak et al. 2019a). Earlier it was shown that the natural mordenite-clinoptilolite rock of Transcarpathia is quite good (Patrylak et al. 2001a) as a carrier for palladium-coated isomerization catalyst.

Therefore, the purpose of this work was to evaluate the effect of improving the porous structure of the natural Transcarpathian zeolite rock on the efficiency of nickel-containing isomerization catalysts on its basis.

Materials and methods

Materials

Synthesis of the catalysts

Mordenite-clinoptilolite rock (Lipcha village, Transcarpathian region) was an origin for successive modification. The major constituents of the utilized rock are SiO_2 (66%), Al_2O_3 (12%), CaO (3%), Na_2O (1%), K_2O (2%), H_2O (11%).

To start with, natural rock was grounded to a fraction of 0.5–1.0 mm. The sample was treated by ammonium chloride (3 mol dm^{-3}) with a liquid to solid ratio of 3:1 by being boiled at 95–100 °C for 2–3 h in a water bath with stirring. Thus, the obtained ammonium form of natural zeolite was separated by filtration, washed by distilled water from chlorine anions and dried at 100 °C. Ammonium form was converted to the hydrogen one by means of calcination for 2 h at 600 °C in a muffle furnace in the presence of air.

To expand the size of pores of the natural material, the rock was dealuminated by removing structural aluminium from the zeolite lattice with hydrochloric acid. For this purpose, the samples of zeolite hydrogen form were treated by concentrated hydrochloric acid solutions (1, 3 and 5 mol dm^{-3}) at the boiling point of the water bath for 3 h. The ratio of solid to liquid phase was 1:3. The obtained samples were filtered off, washed with distilled water until neutral reaction and dried at 100 °C. Thus, samples HMLP-1, HMLP-3 and HMLP-5 were obtained.

The samples were impregnated by nickel. The metal nominal loading for the samples obtained were 1.0, 1.5, 2.0, 2.5, 3.0 wt%. It was assumed that the use of nickel is 100%. Nickel-containing samples were prepared by wetness impregnation using 0.6 mol dm^{-3} solution of nickel (II) nitrate hexahydrate. The solution was evaporated for 12 h at ambient conditions. Then the samples were dried for 2 h at 100 °C. As a result, catalysts with different nickel content were synthesized. Nickel recovery was carried out in a hydrogen flow at 380 °C for 6 h. The amount of nickel in the samples is indicated before the symbol Ni.

Methods

Characterization of the samples

Porous characteristics of the synthesized samples have been found via low-temperature (-196 ºC) nitrogen adsorption/desorption isotherms measured using Nova 1200e (Quantochrome) porometer. The specific surface areas (S_{BET}) have been calculated according to the standard Brunauer–Emmet–Teller (BET) method utilizing the nitrogen adsorption data at P/P_0 values between 0.06 and 0.2 (Rouqerol et al. 1999). The micropores volumes (V^t_{micro}) and micropores surface areas (S^t_{micro}) have been estimated using the de Boer t-plot method. Nitrogen of high purity (99.99%) was used in adsorption measurements.

X-ray diffraction studies with standard measurement on «D8 ADVANCE» Bruker diffractometer with the Ni filtered CuKα radiation (λ = 1.542 nm) in a reflected beam at the Bragg–Brentano focus geometry in the range 2θ = 3–80° with a step of 0.03° and 1 s exposure has been used.

Zeolite silica-to-alumina ratios in the synthesized samples have been determined using X-ray fluorescence analysis (X-Supreme8000 Oxford Instruments).

High performance, high contrast, 40–120 kV transmission electron microscope JEM-1230 with excellent imaging capabilities suitable for chemical and materials science applications has been used for investigation of nickel particles size distribution and their shape.

Vibrational spectroscopies, in particular, IR spectroscopy have played a great role in the characterization of natural and synthetic zeolite materials. IR-spectra of zeolites in the region of framework vibration (400–1500 cm^{-1}) were recorded with a Shimadzu IR Affinity-1S FTIR spectrometer. The spectral resolution was 2 cm^{-1}.

Lewis and Brønsted acidity of the samples were investigated using pyridine as a spectral probe with IR-spectroscopic control. The IR-spectra were obtained using the Spectrum One FTIR-spectrometer (Perkin–Elmer) in the range 1250–4000 cm^{-1}. The samples were pressed into the tablets of 1–9 mg weight and an area of 0.000064 m^2 without binder and loaded into a special holder, designed for four samples. Then, the latter was loaded into a spectral cell and the samples have been activated in a vacuum at 430–450 ºC for 1 h. Thereafter, IR-spectra of vacuumed samples were recorded.

Adsorption of the spectral probe at a temperature of 150 ºC was carried out for 30 min. To determine the zeolite acid site strength the pyridine desorption at 250 ºC for 30 min was carried out, following IR-spectra recording. Transmission spectra were converted to absorption spectra using Spectrum v.5.3 software.

Simultaneous thermogravimetric (TG) and differential thermal analysis (DTA) of the samples were carried out using Linseis STA 1400 system type derivatograph at heating rate of 10 °C min^{-1} in the temperature range 20–1000 °C. Alumina calcined at 1200 °C was used as reference material. All determinations were carried out under normal atmospheric conditions. Approximately 25 mg of sample was used in each experiment.

Catalytic tests

Catalytic properties of the nickel-containing samples obtained have been studied in linear hexane isomerization using micro pulse setup based on gas chromatograph equipped with a flame ionization detector (Patrylak et al. 2019a, 2003; Patrylak 2020). The process was investigated at 200–350 °C with a step of 50 °C. High purity hydrogen (99.99%) was utilized as the carrier gas. The catalyst sample (100 mg) was dehydrated in a hydrogen flow (0.5 l h^{-1}) with increasing (20 ºC min^{-1}) reactor temperature up to 500 ºC, followed by exposure of the sample to this temperature for 1 h. Analytical grade *n*-hexane has been injected by means of pulses of 1 µl using micro syringe in the hydrogen stream (10 ml min^{-1}). The reaction products and unconverted *n*-hexane were collected in a trap cooled by liquid nitrogen (− 196 °C) and in situ analyzed after being vaporized by a thermal impulse of 200 °C. The capillary column (50 m, 0.25 mm inner diameter) with squalane as the stationary phase has been used. The temperature in the column thermostat was 50 °C.

The main isomerization products were 2-methylpentane (2-MP), 3-methylpentane (3-MP), 2,2-dymethylbutane (2,2-DMB) and 2,3-dymethylbutane (2,3-DMB). Cracking products such as methane, ethane, propane, *n*-butane and *n*-pentane have been detected also. Moreover, the *iso*-butane and *iso*-pentane has been found in the reaction products.

Results and discussions

Catalyst characterization

According to the XRD pattern (Fig. 1), the crystalline raw material is represented by the phase of mordenite and clinoptilolite with mica admixtures. A number of characteristics peaks for mordenite and clinoptilolite zeolites (2θ = 6,5;

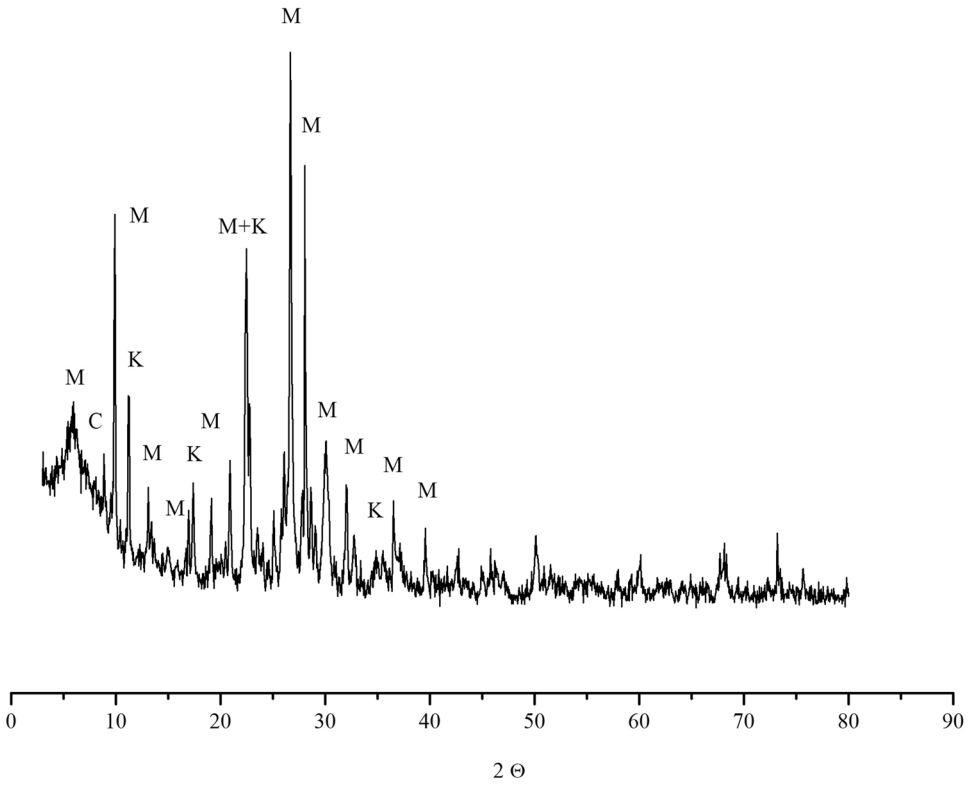

Fig. 1 X-ray diffraction evidences of the natural zeolite rock: M—mordenite, K- clinoptilolite, C – mica

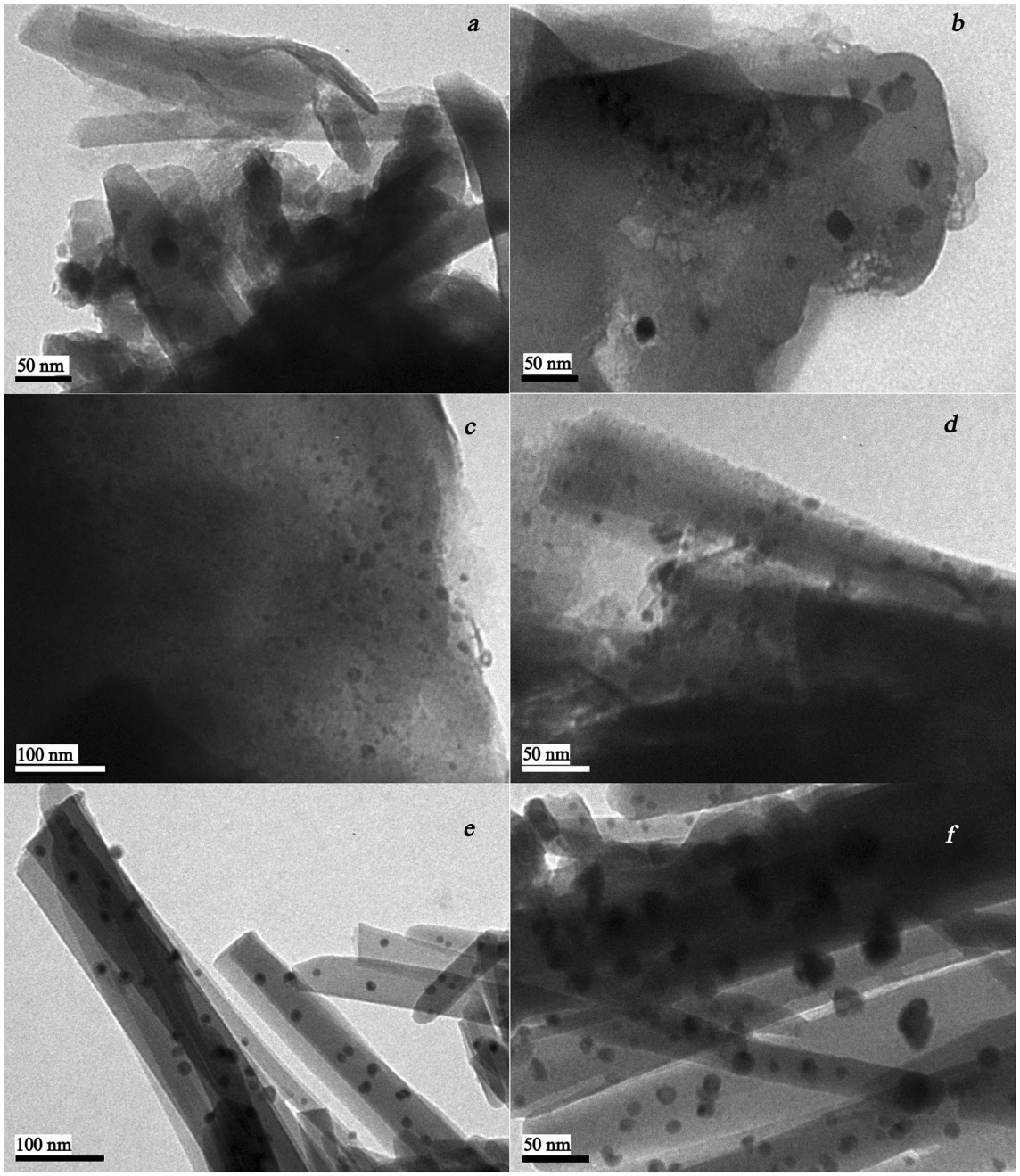

Fig. 2 TEM images of nickel nanoparticles over zeolite samples with different metal content: **a**, **b** HMLP-1-1Ni; **c**, **d** HMLP-1-2Ni; **e**, **f** HMLP-1-2.5Ni

9,76; 13,44; 13,82; 14,58; 19,6; 22,18; 23,14; 25,6; 26,22; 27,66; 33,12; 35,58°) were identified (Treacy and Higgins 2001; Sánchez-López 2019). The XRD analysis shows that mordenite is the main mineral in the sample. The content of mordenite and clinoptilolite is 75 and 25 wt%, respectively.

TEM images for sample HMLP-1-1Ni (Fig. 2) demonstrate significant dispersion of nickel particles by dimensions. This sample has metal nanoparticles with typical species sizes ranging from 20 to 60 nm. HMLP-3-1Ni catalyst is characterized by rather mono-dimensional metal particles of 10–15 nm (Fig. 3). The classical elongated mordenite crystals (Ruiz-Baltazar et al. 2015; Issa et al. 2019) are clearly visible in the micro photos of this sample. They are also present in an image of HMLP-1-2.5Ni (Fig. 2e, f)

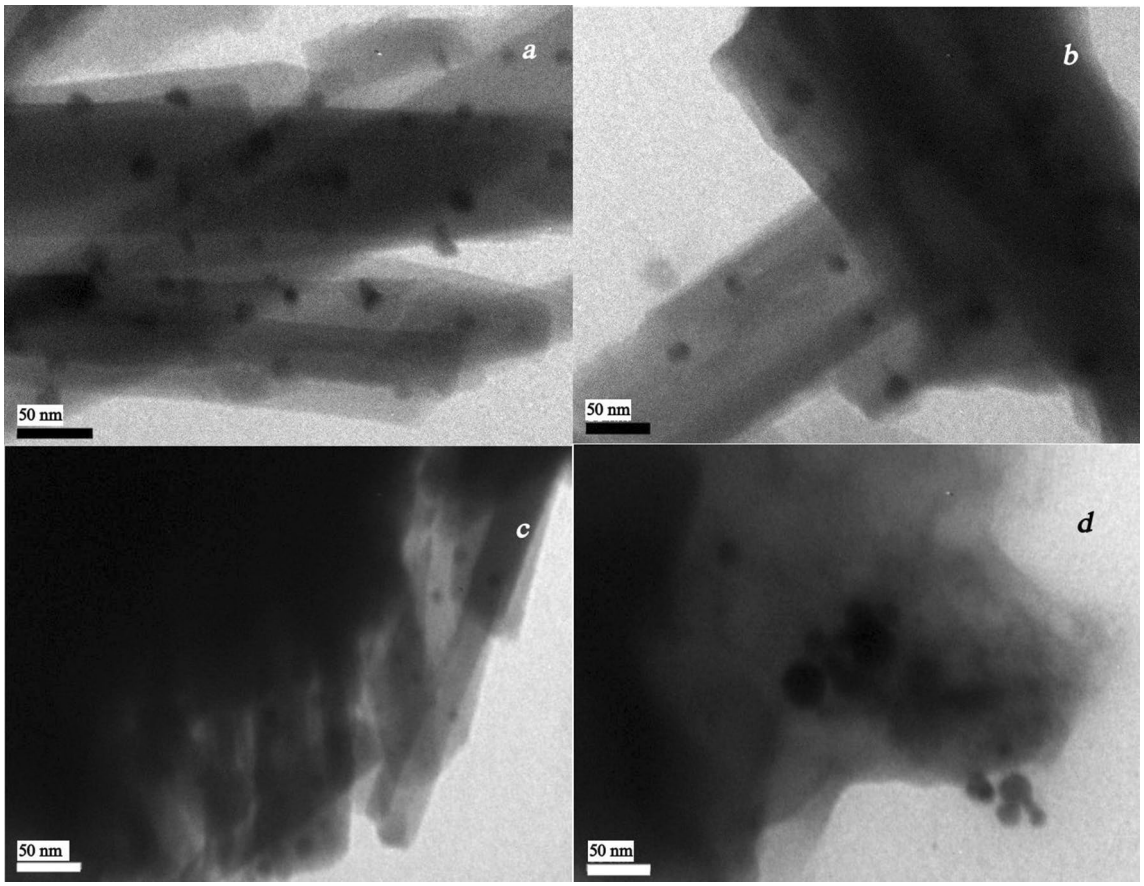

Fig. 3 TEM images of metal nanoparticles over zeolite samples with 1 wt% of nickel treated with acid solutions of different concentrations: **a**, **b** HMLP-3-1Ni; **c**, **d** HMLP-5-1Ni

Table 1 Characteristics of nickel specimens over the catalysts

Catalyst	Species size, nm	Description of metal particles
HMLP-1-1Ni	10–60	Significant particle size distribution
HMLP-1-2Ni	5–8, 12, 15	Many small particles 5–8 nm, few 12, 15 nm
HMLP-1–2.5Ni	10–15, 20–40	Many particles 10–15 nm, few 20–40 nm
HMLP-3-1Ni	10–15	Slight variation in particle size
HMLP-5-1Ni	10, 50	Most particles are 10 nm, some are 50 nm

and HMLP-5-1Ni sample (Fig. 3c). But, the last catalyst has no such uniqueness in the size of nickel crystallites—in addition to 10 nm species larger agglomerates of the order of 50 nm are also found. Samples treated with 1 mol dm^{-3} acid are characterized by a large number of small particles of 5–8 nm for HMLP-1-2Ni and of 10–15 nm for HMLP-1-2.5Ni with segregate larger ones. Table 1 summarizes the results of TEM investigations of the nickel-containing catalysts.

XRF results show that SiO_2 and Al_2O_3 are the main components of the samples. The native exchange cations are Ca, K and Na. The silica-to-alumina ratio of the original material indicated by the XRF analysis was 18.4, whereas acid treated samples had SiO_2/Al_2O_3 ratios of 24.6, 26.6 and 30.2 for 1, 3 and 5 mol dm^{-3} acid concentrations, respectively.

It is well known that the major structural groups present in zeolites can be detected from their mid-infrared pattern (Mikuła et al. 2018). The change of the silica-to-alumina ratio, as a result of the partial removal of aluminum from the structure, reflects the shift of absorption bands of antisymmetrical valence vibrations of (Si, Al)–O bond at 1026 cm^{-1} for the raw rock into the high-frequency region (Fig. 4). For

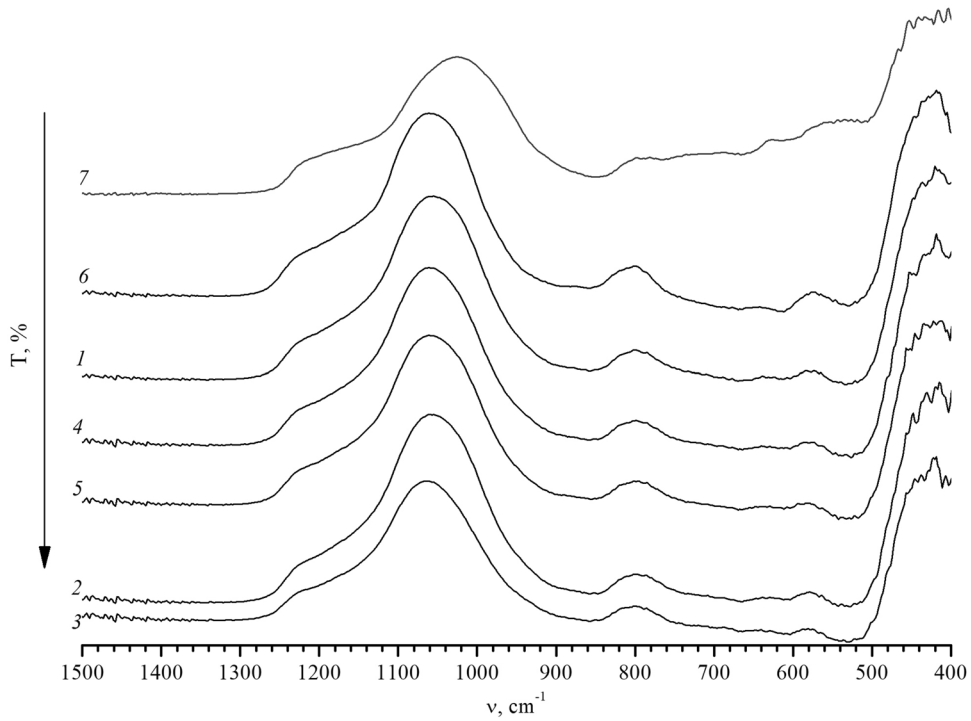

Fig. 4 FTIR-spectra of investigated samples: 1—HMLP-1-1Ni; 2—HMLP-1-1.5Ni; 3—HMLP-1-2Ni; 4—HMLP-3-1Ni; 5—HMLP-5-1Ni; 6—HMLP-1-2.5Ni; 7—HMLP

samples HMLP-1-1Ni, HMLP-3-1Ni and HMLP-5-1Ni treated with 1, 3, and 5 mol dm^{-3} acid solutions, in particular, a band shift up to 1055 cm^{-1} and up to 1061 cm^{-1} was observed. This is consistent with the postulate of Woiciehovska et al. (2019)—the higher Si/Al ratios, the band-specific ring oscillations shift towards higher frequencies.

The shift of the band, which characterizes the absorption in the double ring, to the high frequency region is also noticeable. The initially blurred band at 518–550 cm^{-1} shifts to 573–578 cm^{-1} and 584–592 cm^{-1} with an increased acid concentration. It is less when high-frequency shift characteristic of deformation vibrations of tetrahedrons is at 420 cm^{-1}. When symmetric valence vibrations are at 630 cm^{-1}, reflecting vibrations within tetrahedra, they are not sensitive to changes in the structure of the framework within one type of zeolite, and therefore do not change. The shoulders at 1260 cm^{-1} indicate the existence of mordenite with the accompanying crystalline phase of clinoptilolite.

If the content of metal (nickel) in the samples of the same acid treatment increases (curves 1–3), there is also some shift of the frequency of the band in the region of 1050 cm^{-1} to the high-frequency region from 1055 to 1063 cm^{-1}.

IR spectroscopy is used to determine the O−H bond strength by the direct measurement of the ν(OH) stretching frequency (Borgida et al. 2015): the higher the ν(OH) is, the stronger is the O−H bond, the Al−O−H zeolitic site is less inclined to release H^+ to an adsorbed base, and consequently, the Brønsted acidic strength of the center is lower.

In Fig. 5, the IR-spectra in the field of OH-groups valence vibrations of the original rock in hydrogen form and samples treated by acid are depicted. If the dealumination degree of zeolite samples increases, the bands at 3610, 3650, and 3750 cm^{-1} become clearer and their intensity increases. Both the first and second bands of lower frequencies are generally oscillations of the OH-groups of isolated Brønsted acid centers located in the 12-membered ring channels (Borgida et al. 2015), moreover the acidic centers, which correspond to the first band, are stronger. The band at 3750 cm^{-1} responds to vibrations of non-acidic silanol Si–OH groups (Borgida et al. 2015). Usually, all zeolites exhibit this peak, a sharp maximum, in a very narrow interval independently on the zeolite topology and on the silica-to-alumina ratio.

During the sorption of pyridine on the evacuated samples, characteristic absorption bands in the region of the adsorbed pyridine were recorded (Fig. 6). The coordinate bonded pyridine with Lewis acid site (LAS) signals at 1450 cm^{-1}, whereas the pyridinium ion formed by interaction with the Brønsted acid site (BAS) signals at 1550 cm^{-1} (Patrylak 1999; Kondo et al. 2010; Lukyanov et al. 2014; Phung and Busca 2015). Both bands are clearer and more intense with acid treated samples. If the ratio of the bands intensity is approximately 1:1 for the initial HMLP and HMLP-1

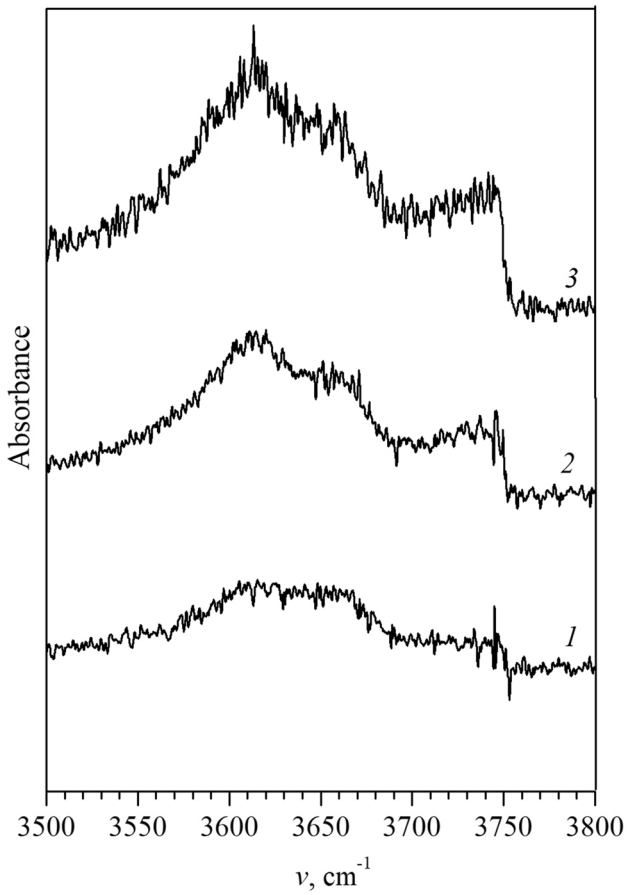

Fig. 5 IR-spectra of raw rock in H-form (1), samples treated by 1 and 3 mol dm^{-3} of hydrochloric acid HMLP-1-1Ni (2), and HMLP-3-1Ni (3) in the range of valence vibrations of OH-groups

samples, meaning that the ratio of BAS to LAS is the same as well, then, when the acid concentration is increased to 3 mol dm^{-3}, the predominance of LAS (1450 cm^{-1}) is manifested. The increase of LAS evidently happens due to the formation of extraframework aluminum. To the latter A.Corma attributed a positive role in the isomerization process. According to Corma et al. (1991), the availability of small amounts of extraframework aluminum increases the activity of the dealuminated synthetic mordenite for the pentane isomerization. It seems that when treated with acid, the strength of acid centers increases, as pyridine desorbed poorely from samples. A significant difference between the spectra of samples with 1 and 2 wt% nickel content was not observed.

It is known that natural zeolites are microporous crystalline aluminosilicates that possess well-ordered open pores in the form of regular channels and cavities of molecular dimensions. The textural characteristics of the synthesized samples obtained by low-temperature adsorption/desorption of nitrogen are summarized in Table 2. The initial raw MLP sample has a relatively low BET specific surface area of pores 95 m^2g^{-1} (Table 2), which is approximately the same as the other results for natural zeolite rocks (Korkuna et al. 2006; Selvam et al. 2018). Whereas, the surface of faujasite zeolites obtained in situ from kaolinite were significantly higher and reaches up to 250–300 m^2 g^{-1} (Patrylak et al. 2001b, 2019b). BET surface of the mordenite-clinoptilolite samples significantly increased as the result of further modification by acid. After treatment with 1 mol dm^{-3} acid and the metal doping, the BET surface increases to 300 m^2 per gram, which is close to the values for synthetic mordenite type zeolite (HM-1Ni, $SiO_2/Al_2O_3 = 19.6$) (Patrylak 2020). The volume of micropores in the investigated samples increased approximately four times. The latter can be caused not only by the removal of structural aluminum, but also by the replacement of the original sodium, potassium and calcium cations of starting material by a smaller proton cation. The volume of mesopores with a diameter of 2 to 10 nm, calculated by the BJH method, also doubled (Table 3) in the case of acid treatment by 1 and 3 mol dm^{-3} HCl, despite the additional impregnation by nickel. Moreover, treatment with more concentrated acid (5 mol dm^{-3} HCl) leads to tripling the volume of mesopores.

The original form of the mordenite-clinoptilolite rock MLP, as well as the samples HMLP-1-1.5Ni and HMLP-1-2Ni were investigated using the DTA/TG method. In Fig. 7, the corresponding curves are shown. It is known that the loss of water from the zeolite samples generally occurs in the temperature range 100–400 °C and it is manifested in the DTA graphs by an extended endothermic effect (Afzal et al. 2000; Mansouri et al. 2013).

The DTA curves of the original rock MLP, HMLP-1-1.5Ni and HMLP-1-2Ni samples are characterized by endotherms near 100 °C related to the dehydration process. The dehydration rate is substantially higher in the temperature range up to 200 °C in the case of modified samples (Table 4), in comparison with the original sample. This is caused by pores enlargement as a result of acid treatment. Which, therefore, quickens the dehydration process. Peculiarities of dehydration are attributed to the difference in the bonding strength of the water molecules in the zeolite. Physically sorbed or mobile water on the surface and in the pores is removed at temperatures up to 100 °C and up to 200 °C from lager and narrower cavities, respectively. Immobile or zeolite structure water in the pores is removed at 500–800 °C. The last one causes a change in Brønsted

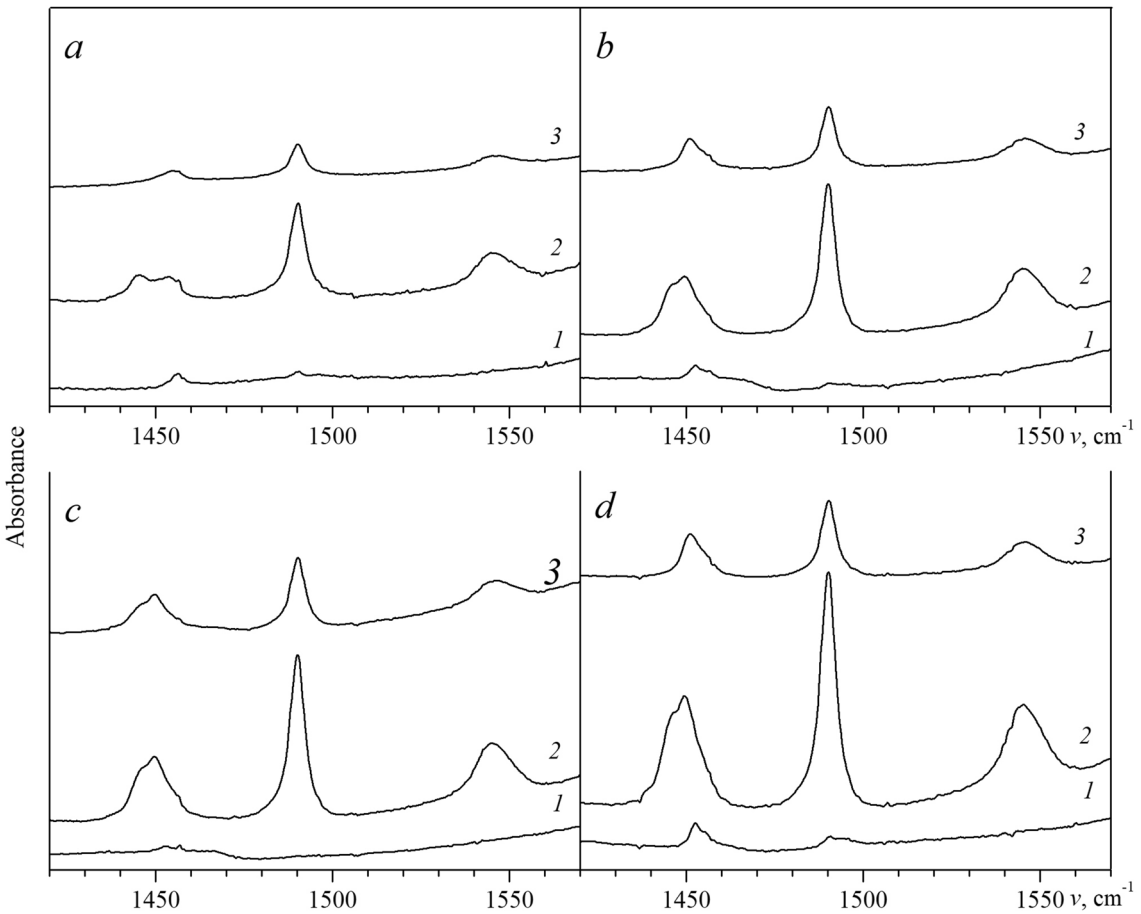

Fig. 6 IR-spectra of HMLP (**a**), HMLP-1-1Ni (**b**), HMLP-1-2Ni (**c**) and HMLP-3-1Ni (**d**) in the region of adsorbed pyridine: 1—vacuumed samples before adsorption, 2—after pyridine adsorption at 150 °C, 3—after pyridine evacuation at 250 °C

Table 2 Adsorption characteristics of nickel-modified samples of acid-treated zeolite rocks

Sample	S^{BET}, $m^2\ g^{-1}$	S^t, $m^2\ g^{-1}$	S^t_{micro}, $m^2\ g^{-1}$	V_Σ, $cm^3\ g^{-1}$	V^t_{micro}, $cm^3\ g^{-1}$	V_{micro}/V_Σ, %	R^{DFT}, nm	R, nm
MLP	95	25.4	69.9	0.099	0.032	32.3	1.173	2.09
HMLP-1-1Ni	330	32.0	298	0.204	0.133	65.2	1.173	1.237
HMLP-1-1.5Ni	304	30.0	274	0.189	0.121	64.0	1.173	1.243
HMLP-1-2Ni	287	30.0	257	0.182	0.116	63.7	1.173	1.267
HMLP-1-2.5Ni	278	50.6	228	0.215	0.116	54.0	1.173	1.541
HMLP-1-3Ni	301	40.1	261	0.211	0.124	58.8	1.173	1.400
HMLP-3-1Ni	292	33.0	259	0.186	0.117	62.9	0.807	1.272
HMLP-5-1Ni	322	37.9	284	0.212	0.113	53.3	1.252	1.318
HM-1Ni [38]	336	16.5	319	0.172	0.132	0.040	1.173	1.025

Table 3 The volume of mesopores of 2–10 nm diameter, calculated by BJH method, for initial and modified samples

Samples	Volume of mesopores, $cm^3\ g^{-1}$	
	ads	des
MLP	0.020	0.020
HMLP-1-1Ni	0.040	0.035
HMLP-1-1.5Ni	0.035	0.035
HMLP-1-2Ni	0.040	0.038
HMLP-1-2.5Ni	0.070	0.070
HMLP-1-3Ni	0.050	0.055
HMLP-3-1Ni	0.045	0.040
HMLP-5-1Ni	0.065	0.055

acidity of zeolite. At high temperatures, the dehydroxylation of the Brønsted acid site occurs with appearance of Lewis acid site and water molecule.

Mordenite and clinoptilolite zeolites belong to a group of natural minerals that do not show major structural changes at 800–900 °C. They remain stable during the dehydratation processes. A phase transition process without loss of mass is observed at temperatures close to 800 °C for the raw rock only. The corresponding thermogravimetric curve shows that weight loss is generally observed up to 600 °C and afterwards there is no weight change. The detected exothermic energy change is due to the phase changes that occur in alumina-silica system. Data of the thermal analyses are in agreement with the results of Alver et al. (2010), where the natural and modified clinoptilolite structure remained unchanged up to 700 °C.

The total mass loss for all the samples was essentially the same. However, as shown in Table 4, the raw material loses all physisorbed water at temperatures up to 600 °C, whereas modified samples loss adsorbed water more quickly, but retain the structural water at temperatures up to 800 °C. The last process is indicated by the slight slope of the TG curve in the high temperature region, which displays the existence of strong Brønsted acid sites in the modified samples.

Catalytic investigations

Three samples of natural zeolite rock with 1 wt% nickel content practically do not differ in linear hexane conversion (Fig. 8a). At the same time, the yield of isomeric structures stands out for the sample treated with 1 mol dm^{-3} hydrochloric acid (Fig. 8b), for which the maximum yield of 14% is fixed at 300 °C. However, it significantly drops from 75% at 250 °C to 50% at 275 °C and to 40% at 300 °C. Starting at 300 °C, the cracking rate increases significantly, which, for samples HMLP-3-1Ni and HMLP-5-1Ni, proceeds with more than 90% selectivity. Taking into account that all three samples contain nickel particles of 10 nm in size, it appears, the size of the nickel crystallites in the samples of this range is not determinative, although in research (Patrylak 2019a), the best catalytic properties were shown by ZSM-5 zeolite catalyst with small nickel particles of 8–9 nm. Obviously, the acid treatment had a more significant effect. Increasing the concentration of hydrochloric acid causes a greater removal of structural aluminum from the zeolite lattice with the appearance of more structural defects. On one hand, it was supposed to increase the acid strength of the Brønsted acid sites as the silica-to-alumina ratio rises, but on the other hand, it reduced their number and widened the pore size, destroying the structure. Apparently, the use of 1 mol dm^{-3} hydrochloric acid was sufficient to partially expand the pores while not reducing the number of acid centers too significantly. The relatively small yields of isomers on these samples are explained by the micro-pulse conditions of the test.

The increase in nickel content up to 2 wt% had a positive effect on the main reaction proceeding (Fig. 9). For the HMLP-1-1.5Ni and HMLP-1-2Ni samples, the maximum of the yield of isomeric structures in the region of lower temperatures is shifted to 250 and 275 °C, respectively, and the yield of *iso*-hexanes increases up to 20%. Moreover, the selectivity for branched structures of the sample with 2 wt% nickel at 250 °C is 70%, i.e., the yield of the products of cracking is low. However, a further increase in the nickel content to 2.5 and 3 wt% had a negative effect on the isomerization activity of the samples due to the resulting cracking.

These results are superior to those obtained during catalytic tests for samples of synthetic microporous zeolite 0.5PdHM (Patrylak 2003) and HM-1Ni (Patrylak 2020), which are characterized by yields of 18% and 11% at 340 and 300 °C, respectively. The increase in the nickel content to 5 wt% was contributed to the shift of the maximum at the isomer yield in the range of lower temperatures (up to 250 °C), but the yield was still practically unchanged (12%) (Patrylak 2020).

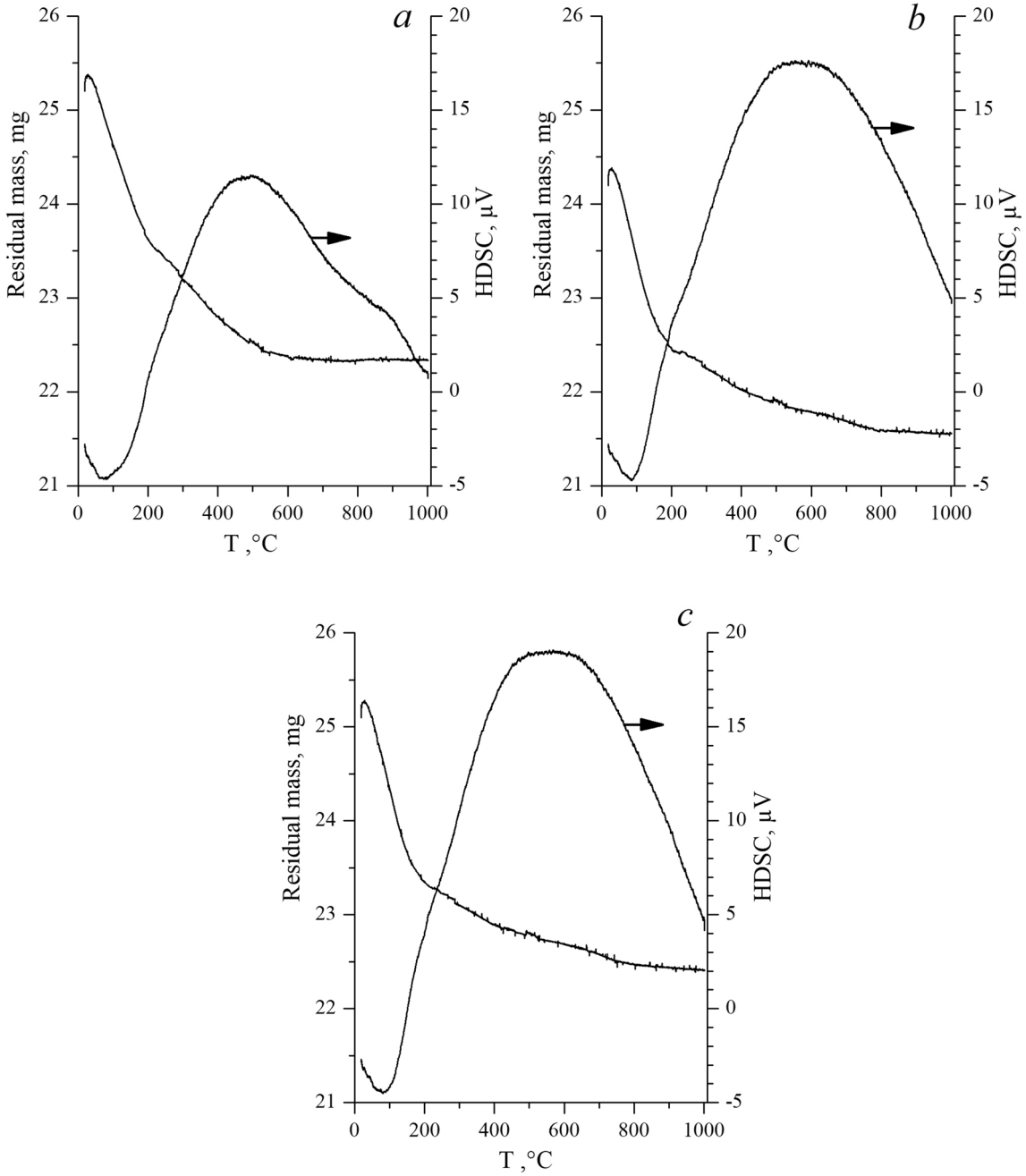

Fig. 7 DTA and TG results for original zeolite rock MLP (**a**), nickel-containing samples HMLP-1-1.5Ni (**b**), and HMLP-1-2Ni (**c**)

Table 4 Mass loss (%) for samples at different temperature ranges

Sample	Temperature, °C			
	20–200	200–600	600–800	Total
MLP	7.1	4.7	-	11.8
HMLP-1-1.5Ni	8.2	2.5	1.2	11.5
HMLP-1-2Ni	7.8	2.3	1.2	11.3

If we analyze the composition of the conversion products in more detail (Table 5), it should be noted that in addition to 2-MP and 3-MP, 2,2-DMB in quantities up to 2% were recorded under micro-pulse conditions. Moreover, *iso*-butane and *iso*-pentane (up to 5–7%) were detected among the products that were marked as products of cracking. The latter are formed from linear cracking products, but they are

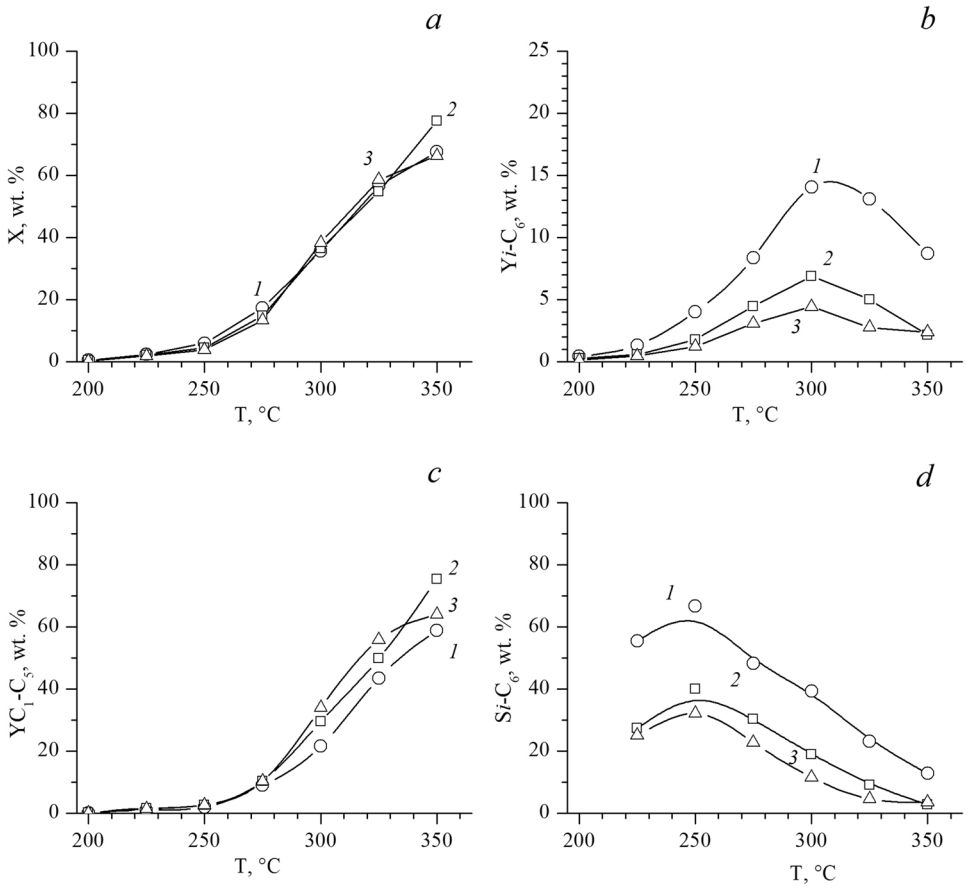

Fig. 8 Conversion of *n*-hexane (**a**), yield of *i*-C_6 (**b**), yield of cracking products C_1-C_5 (**c**), and selectivity to *i*-C_6 (**d**) for synthesized zeolite samples of acid treatments: HMLP-1-1Ni (1), HMLP-3-1Ni (2), HMLP-5-1Ni (3)

isomeric structures, and, therefore, can be attributed to the target products of isomerization. Thus, the yield of all *iso*-structures for the sample HMLP-1-2Ni with 2 wt% of nickel was 30% at 275 °C.

Like nickel-containing ZSM-5 samples, the sample with the smallest particle size of nickel (5–8 nm) is the most active.

Conclusions

Physico-chemical and catalytic investigations of natural Ukrainian zeolite samples treated by hydrochloric acid with nanosized nickel particles have shown the following consequences:

- the low-temperature nitrogen adsorption/desorption has indicated that, despite additional modification by metallic component, acid treatment of natural zeolite rock increases the volume of mesopores by 2–3 times and the volume of micropores up to four times;
- X-ray fluorescence analysis and FTIR spectroscopy confirmed the increase of the silica-to-alumina ratio in samples during the process of acidic dealumination of the zeolite structure;
- pyridine sorption with IR-spectroscopic control shows the presence of Brønsted and Lewis acid sites over catalysts. For the HMLP sample and for the sample treated by 1 mol dm^{-3} acid solution, the ratio of Brønsted/Lewis acid sites practically equals to 1, but the application of stronger acid solutions leads to the predominance of Lewis acidity;

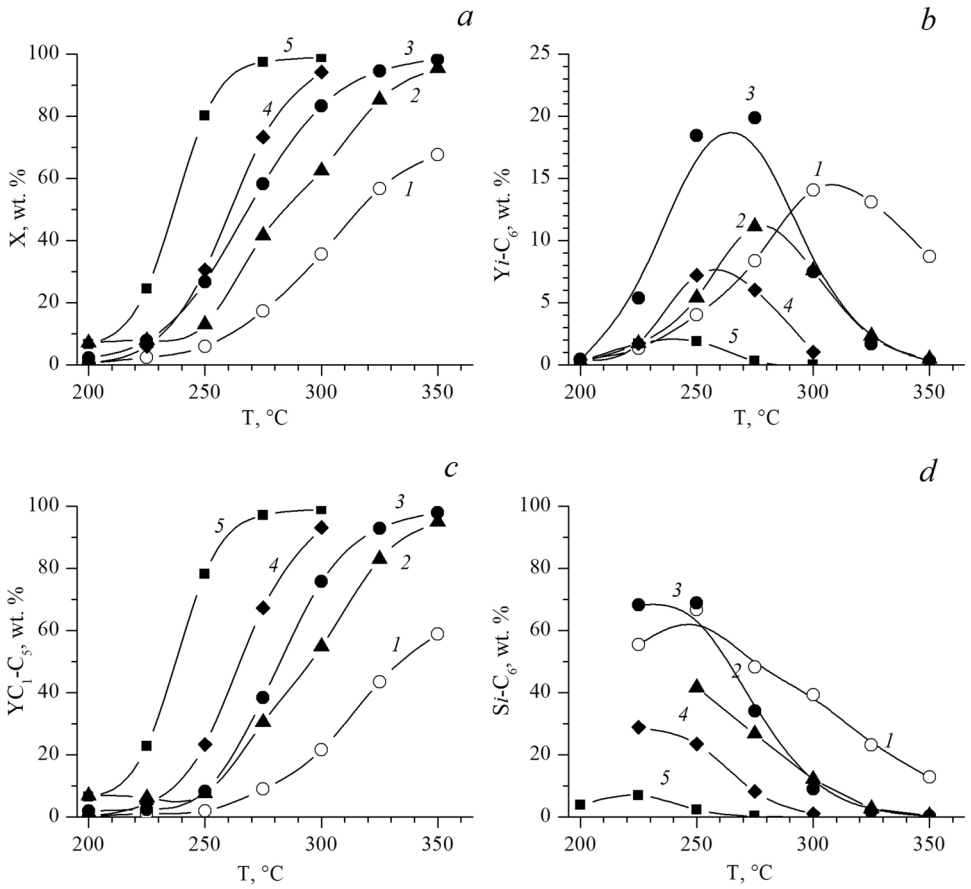

Fig. 9 Conversion of *n*-hexane (**a**), yield of *i*-C_6 (**b**), yield of cracking products C_1-C_5 (**c**), and selectivity to *i*-C_6 (**d**) for the zeolite samples with different nickel content: HMLP-1-1Ni (1), HMLP-1-1.5Ni (2), HMLP-1-2Ni (3), HMLP-1-2.5Ni (4), HMLP-1-3Ni (5)

- the size of metal crystallites deposited on the natural zeolite rock surface after preliminary acid dealumination has been estimated. The latter is 10 nm for most samples, but larger units up to 20–50 nm and smaller particles of about 5 nm were also observed;
- DTA/TG investigations show different peculiarities of physisorbed water removing from pores of the original zeolite rock and from the samples with enlarged cavities after acid treatment. Structural zeolite water in the form of Brønsted acid sites is removed at 500–800 °C;
- nickel-modified catalysts were tested for isomerization of linear hexane in a flow micro-pulse mode in a hydrogen stream. The sample with 2 wt% nickel content and the smallest metal nanoparticles of 5–8 nm showed the best performance (20% yield of C_6 isomers at 250 °C), which is higher than the microporous nickel-containing synthetic mordenite zeolite (12% at 300 °C).

Table 5 Composition of linear hexane isomerization products

Sample/Temperature, °C	Content, wt%										
	CH_4	C_2H_6	C_3H_8	*i*-C_4H_{10}	*n*- C_4H_{10}	*i*-C_5H_{12}	*n*-C_5H_{12}	2,2-DMB	2MP	3MP	*n*-C_6H_{14}
HMLP-1-1Ni											
250	0.08	0.50	0.44	0.47	0.19	0.25	0.08	0.24	3.78	0	93.98
275	0.49	0.50	2.73	0.60	2.90	1.38	0.38	0.66	7.73	0	82.63
300	1.89	0.96	7.41	2.18	5.48	2.76	0.93	1.06	8.96	4.03	64.34
HMLP-3-1Ni											
250	0.23	0.95	0.47	0.21	0.29	0.13	0.40	0.17	1.62	0	95.54
275	2.17	0.90	2.19	1.05	1.56	0.66	1.75	0.34	3.42	0.74	85.23
300	8.91	1.99	6.67	2.32	4.25	1.69	3.83	0.54	4.41	1.95	63.45
HMLP-5-1Ni											
250	0.47	0.72	0.36	0.13	0.24	0.09	0.59	0	1.23	0	96.17
275	2.77	0.80	1.99	0.64	1.50	0.43	2.28	0	3.09	0	86.50
300	11.14	2.56	6.42	1.01	5.54	0.99	6.31	0	4.45	0	61.58
HMLP-1-1.5Ni											
250	2.93	1.06	0.75	0.20	0.75	0.32	1.56	0	5.16	0	87.03
275	12.76	2.27	3.88	0.73	4.16	1.39	5.27	0.61	7.15	3.36	58.41
300	28.70	5.18	7.48	1.67	4.81	1.78	5.22	0.60	4.62	2.37	37.56
HMLP-1-2Ni											
250	3.09	0.65	0.64	0.25	0.87	0.93	1.90	0.56	12.38	5.53	73.21
275	14.81	2.21	5.32	2.14	4.07	4.66	5.20	1.31	12.42	6.16	41.69
300	38.62	7.72	9.38	2.57	9.19	3.62	4.71	0.80	4.21	2.49	16.71
HMLP-1-2.5Ni											
250	9.99	1.17	1.56	0.87	2.97	1.6	5.24	0	5.3	1.91	69.39
275	34.63	3.99	7.94	1.37	9.44	1.94	7.96	0.62	3.58	1.83	26.69
300	22.68	49.18	10.85	1.17	6.24	0.66	2.39	0.25	0.47	0.31	5.78
HMLP-1-3Ni											
250	38.65	4.68	11.28	5.18	5.72	1.04	11.71	0	1.21	0.71	19.83
275	68.83	10.93	13.68	1.16	6.79	0.35	2.41	0	0.2	0.13	2.53
300	44.76	44.65	6.94	0.72	1.26	0.12	0.49	0	0	0	1.06

Acknowledgements The authors acknowledge the assistance and support of M.G. Kholodny Institute of Botany of National Academy of Sciences in conducting the electron transmission microscopy experiments. The publication contains the results of studies conducted by President's of Ukraine grant for competitive projects F84/147-2019 and by grant of National Research Fundation of Ukraine project 2020.01/0042.

Compliance with ethical standards

Conflict of interest On behalf of all authors, the corresponding author states that there is no conflict of interest.

References

Afzal M, Yasmeen G, Saleem M, Butt PK, Khattak AK, Afzal J (2000) TG and DTA study of the thermal dehydration of metal-exchanged zeolite-4A samples. J Therm Anal Calorim 62:721–727. https://doi.org/10.1023/A:1026725509732

Alver BE, Sakizci M, Yörükoğullari E (2010) Investigation of clinoptilolite rich natural zeolites from Turkey: a combined XRF, TG/DTG, DTA and DSC study. J Therm Anal Calorim 100:19–26. https://doi.org/10.1007/s10973-009-0118-0

Bai R, Song Yu, Li Y, Yu J (2019) Creating hierarchical pores in zeolite catalysts. Trends Chem 1:601–611. https://doi.org/10.1016/j.trechm.2019.05.010

Bordiga S, Lamberti C, Bonino F, Thibault-Starzyk F (2015) Probing zeolites by vibrational spectroscopies. Chem Soc Rev 44:7262–7341. https://doi.org/10.1039/C5CS00396B

Corma A, Frontela J, Lazaro J, Perez M (1991) Alkylation, Aromatization, Oligomerization and Isomerization of Short Chain Hydrocarbons over Heterogeneous Catalysts. In: W.E. Haines (eds) Preprints Div. Petrol. Chem., ACS Symposium Series, vol. 36, New York, p. 833.

Devaraj A, Vijayakumar M, Bao J, Guo MF, Derewinski MA, Xu Z, Gray MJ, Prodinger S, Ramasamy KK (2016) Discerning the location and nature of coke deposition from surface to bulk of spent zeolite catalysts. Sci Rep 6:37586. https://doi.org/10.1038/srep37586

Feliczak-Guzik A (2018) Hierarchical zeolites: Synthesis and catalytic properties. Microp Mesopor Mater 259:33. https://doi.org/10.1016/j.micromeso.2017.09.030

Jordao MH, Simoes V, Cardoso D (2007) Zeolite supported Pt-Ni catalysts in *n*-hexane isomerization. Appl Catal A 319:1–6. https://doi.org/10.1016/j.apcata.2006.09.039

Khan W, Jia X, Wu Z, Choi J, Yip ACK (2019) Incorporating hierarchy into conventional zeolites for catalytic biomass conversions: a review. Catalysts 9(2):127–150. https://doi.org/10.3390/catal9020127

Kondo JN, Nishitani R, Yoda E, Yokoi T, Tatsumi T, Domen KA (2010) Comparative IR characterization of acidic sites on HYzeolite by pyridine and COprobes with silica–alumina and γ-alumina references. Phys Chem Chem Phys 12:11576–11586. https://doi.org/10.1039/C0CP00203H

Korkuna O, Leboda R, Skubiszewska-Zieba J, Vrublevska T, Gunko VM, Ryczkowski J (2006) Structural and physicochemical properties of natural zeolites:clinoptilolite and mordenite. Microporous Mesoporous Mater 87:243–254. https://doi.org/10.1016/j.micromeso.2005.08.002

Issa H, Chaouati N, Toufaily J, Hamieh T, Sachse A, Pinard L (2019) Toolbox of post-synthetic mordenite modification strategies: impact on textural, acidic and catalytic properties. ChemCatChem 11(18):4581–4592. https://doi.org/10.1002/cctc.201900927

Lima PM, Garetto T, Cavalcante CLJr, Cardoso D, (2011) Isomerization of *n*-hexane on Pt–Ni catalysts supported on nanocrystalline H-BEA zeolite. Catal Today 172:195–202. https://doi.org/10.1016/j.cattod.2011.02.031

Liu B, Slocombe D, AlKinany M, AlMegren H, Wang J, Arden J, Vai A, Gonzalez-Cortes S, Xiao T, Kuznetsov V, Edwards PP (2016) Advances in the study of coke formation over zeolite catalysts in the methanol-to-hydrocarbon process. Appl Petrochem Res 6:209–215. https://doi.org/10.1007/s13203-016-0156-z

Liu Z, Hua Y, Wang J, Dong X, Tian Q, Han Yu (2017) Recent progress in the direct synthesis of hierarchical zeolites: synthetic strategies and characterization methods. Mater Chem Front 1:2195–2212. https://doi.org/10.1039/C7QM00168A

Lukyanov DM, Vazhnova T, Cherkasov N, Casci JL, Birtill JJ (2014) Insights into brønsted acid sites in the zeolite mordenite. J Phys Chem C 118(41):23918–23929. https://doi.org/10.1021/jp5086334

Mansouri N, Rikhtegar N, Panahi HA, Atabi F, Shahraki BK (2013) Porosity, characterization and structural properties of natural zeolite—clinoptilolite—as a sorbent. Env Protec Eng 39:149–152. https://doi.org/10.5277/EPE130111

Martins GSV, dos Santos ERF, Rodrigues MGF, Pecchi G, Yoshioka CMN, Cardoso D (2013) n-Hexane isomerization on Ni-Pt/catalysts supported on mordenite. Modern Res Catal 2:119–126. https://doi.org/10.4236/mrc.2013.24017

Mikuła A, Król M, Mozgawa W, Koleżyński A (2018) New approach for determination of the influence of long-range order and selected ring oscillations on IR spectra in zeolites. Spectrochim Acta A Mol Biomol Spectrosc 95:62–67. https://doi.org/10.1016/j.saa.2018.01.044

Mitchell S, Pinar A, Kenvin J, Crivelli P, Kärger J, Pérez-Ramírez J (2015) Structural analysis of hierarchically organized zeolites. Nat Commun 6:8633. https://doi.org/10.1038/ncomms9633

Na K, Choi M, Ryoo R (2013) Recent Advances in the Synthesis of Hierarchically Nanoporous Zeolites. Micropor Mesopor Mater 166:3–19. https://doi.org/10.1016/j.micromeso.2012.03.054

Nordvang EC, Borodina E, Ruiz-Martínez J, Fehrmann R, Weckhuysen BM (2015) Effects of coke deposits on the catalytic performance of large zeolite H-ZSM-5 crystals during alcohol-to-hydrocarbon reactions as investigated by a combination of optical spectroscopy and microscopy. Chemistry 21(48):17324–17335. https://doi.org/10.1002/chem.201503136

Patrylak LK (1999) Chemisorption of Lewis bases on zeolites—a new interpretation of the results. Adsorpt Sci Technol 17(2):115–123. https://doi.org/10.1177/026361749901700205

Patrylak L, Likhnyovskyi R, Vypyraylenko V, Leboda R, Skubiszewska-Zięba J, Patrylak K (2001a) Adsorption properties of zeolite-containing microspheres and FCC catalysts based on Ukrainian Kaolin. Adsorpt Sci Technol 19(7):525–540. https://doi.org/10.1260/0263617011494376

Patrylak KI, Bobonych FM, Voloshyna YuG, Levchuk MM, Solomakha VM, Patrylak LK, Manza IA, Taranookha OM (2001b) Linear hexane isomerization over the natural zeolite based catalysts depending on the zeolite phase composition. Catal Today 65:129–135. https://doi.org/10.1016/S0920-5861(00)00573-3

Patrylak LK, Manza IA, Vypirailenko VYo, Korovitsyna AS, Likhniovskyi RV, (2003) Study of the mechanism of hexane isomerization under micropulse conditions. Theor Experim Chem 39:263–267. https://doi.org/10.1023/A:1025729530977

Patrylak LK, Pertko OP (2018) Peculiarities of activity renovation of zeolite catalysts coked in hexane cracking. Chem Chem Technol 12(4):538–554. https://doi.org/10.23939/chcht12.04.538

Patrylak LK, Krylova MM, Pertko OP, Voloshyna YuG (2019a) Linear hexane isomerization over Ni-containing pentasils. J Porous Mater 26(3):861–868. https://doi.org/10.1007/s10934-018-0685-1

Patrylak LK, Pertko OP, Povazshnyi VA, Melnychuk OV (2019b) Influence of modification by Zr and La on the porous characteristics and catalytic activity of in situ synthesized microspherical cracking catalysts. Voprosy Khimii i Khimicheskoi Tekhnologii 6:157–163. https://doi.org/10.32434/0321-4095-2019-127-6-157-163

Patrylak L, Krylova M, Pertko O, Voloshyna Yu, Yakovenko A (2020) n-Hexane isomerization over nickel-contaning mordenite zeolites. Chem Chem Technol 14(2):234–238. https://doi.org/10.23939/chcht14.02.234

Phung TK, Busca G (2015) On the Lewis acidity of protonic zeolites. Appl Catal A: Gen 504:151–157. https://doi.org/10.1016/j.apcata.2014.11.031

Rouqerol F, Rouqerol J, Sing K (1999) Adsorption by powders & porous solids: principles. Methodology and applications. Academic Press, San Diego

Ruíz-Baltazar A, Esparza R, Gonzalez M, Rosas G, Pérez R (2015) Preparation and Characterization of Natural Zeolite Modified with Iron Nanoparticles. J Nanomaterials 5:2–8. https://doi.org/10.1155/2015/364763

Wojciechowska KM, Król M, Bajda T, Mozgawa W (2019) Sorption of heavy metal cations on mesoporous ZSM-5 and mordenite zeolites. Materials 12:3271. https://doi.org/10.3390/ma12193271

Sánchez-López P, Antúnez-García J, Fuentes-Moyado S, Galván DH, Petranovskii V, Chávez-Rivas F (2019) Analysis of theoretical and experimental X-ray diffraction patterns for distinct mordenite frameworks. J Mater Sci 54:7745–7757. https://doi.org/10.1007/s10853-019-03407-w

Selvam T, Schwieger W, Dathe W (2018) Histamine-binding capacities of different natural zeolites: a comparative study. Environ Geochem Health 40(6):2657–2665. https://doi.org/10.1007/s10653-018-0129-5

Serrano DP, Pizarro P (2013) Synthesis Strategies in the Search for Hierarchical Zeolites. Chem Soc Rev 42:4004–4035. https://doi.org/10.1039/C2CS35330J

Treacy MMJ, Higgins JB (eds) (2001) Collection of Simulated XRD powder patterns for zeolites. Elsevier, Amsterdam

Weissenberger T, Reiprich B, Machoke AGF, Klühspies K, Bauer J, Dotzel R, Casci JL, Schwieger W (2019) Hierarchical MFI type zeolites with intracrystalline macropores: the effect of the

macropore size on the deactivation behaviour in the MTO reactio. Catal Sci Technol 9:3259. https://doi.org/10.1039/C9CY00368A

Yoshioka CMN, Garetto T, Cardoso D (2005) *n*-Hexane isomerization on Ni-Pt catalysts/supported on HUSY zeolite: The influence from a metal content. Catal Today 107–108:693–698. https://doi.org/10.1016/j.cattod.2005.07.056